JOURNAL OF MATERIALS SCIENCE **35** (2000) 9–14

Mechanical properties of titanium diboride based cermets

J. M. SÁNCHEZ, I. AZCONA, F. CASTRO
Centro de Estudios e Investigaciones Tecnicas de Guipuzcoa (CEIT), Departament of Materials, Paseo Manuel de Lardizábal, 15. 20009. P.O. 1555. San Sebastian, Spain
E-mail: jmsanchez@ceit.es

Mechanical properties of titanium diboride (TiB_2) cermets critically depend on the composition of the binder phase. Both, fracture toughness and hardness are substantially increased by avoiding the formation of extremely brittle secondary borides which form during sintering by chemical reactions between TiB_2 and the metallic additives. Fractographic observations of TiB_2 cermets without secondary borides show the presence of ductile ligaments of the binder phase bridging the advancing crack tip. The powder metallurgy processing route applied to these materials allows modification of the binder phase structure from the ferritic iron-aluminium phase to Fe-Ni-Al austenite by changing the aluminium content of the powder mixtures. The highest toughness values have been obtained for the TiB_2 cermets with an austenitic binder phase. X-ray diffraction analyses of the fracture surfaces of such samples show that the binder phase is metastable exhibiting stress induced martensitic transformation during fracture. This new family of materials presents an outstanding combination of hardness and toughness, comparable to those obtained with commercial grades of tungsten carbide (WC) hardmetals.

1. Introduction

Among the strategies of strengthening and toughening commonly applied to brittle materials, the metal matrix reinforcement has been the most studied route for improving not only the toughness, but also the sinterability of titanium diboride [1–5]. Metals like iron, cobalt and nickel were firstly selected as additives for liquid phase sintering of TiB_2. However, these transition metals react with TiB_2 to form metallic borides of the MB, M_2B and $M_{23}B_6$ types, which are even more brittle than titanium diboride itself [5]. Recent works [6–9] have shown that certain iron-nickel alloys containing controlled additions of Ti and Al can be used as binders for TiB_2 thus preventing the formation of undesirable secondary borides. Chemical compositions of the iron-nickel-based binder phases, whose liquids are in equilibrium with TiB_2 at the sintering temperature, have also been determined by thermodynamic calculations [9]. By following this route, several TiB_2 cermets were produced with different metallic binders.

The objective of this work is to present the most significant mechanical properties of TiB_2 based cermets; i.e. hardness, transverse rupture strength, elastic modulus and, especially, fracture toughness, and to discuss the reinforcing mechanisms observed for the different binder systems.

2. Experimental

2.1. Materials

The characteristics of the basic powders used to prepare the TiB_2-metal mixtures are summarised in Table I.

According to results obtained in previous works [9], three alloys have been selected to study their effect on the mechanical properties of TiB_2 cermets (Table II). Several TiB_2-metal combinations were produced using the above-mentioned alloys with binder volume fractions ranging from 8 to 30%.

Powder mixtures were prepared by ball milling in isopropyl alcohol for 24 h in a polyethylene container with stainless steel balls. Following a conventional powder metallurgy processing route, a set of rigid steel dies was designed to produce the green compacts required for further testing. All test pieces were produced by uniaxial pressing at a constant pressure of 70 MPa (green densities are about 55% T.D.). Full densification of all compositions was achieved by Hot Isostatic Pressing (HIP) at 1350 °C and 150 MPa for 30 min after encapsulation using a glass powder method reported elsewhere [10]. Quality control of selected sintered specimens was carried out by X-Ray Diffraction Analysis (XRD), Electron Microscopy and Light Element Energy Dispersion Spectroscopy.

2.2. Mechanical properties

Vickers Hardness measurements were carried out on cylinders 13 mm in diameter and 5 mm high. Each sample was indented five times using a Tukon indenter at a constant load of 10 kg (HV10). The cracks developed at the corners of the Vickers hardness indentations were used to measure the surface critical stress intensity factor, K_{IC}^{S}, of TiB_2 cermets by applying the

TABLE I Characteristics of the basic powders (provided by the suppliers)

Chemical composition in wt %	B	Fe	Ni	C	O	N	BET (m^2/g)	Mean particle size (μm)	Max. particle size (μm)
TiB_2 (grade F)[a]	>28.5	<0.25	*	<0.25	<2	<0.25	>4	1.5	6
Fe[b]	*	Balance	*	0.023	0.457	0.054	*	2	4
Ni[b]	*	*	Balance	0.075	0.191	0.033	*	2	4
$TiAl_3$[c]	*	*	*	*	*	*	*	10	30

[a]Provided by H. C. Stark (Germany).
[b]Provided by Bonastre S. A. (Spain).
[c]Ti and Al are added to the powder mixtures as the intermetallic $TiAl_3$, provided by Good fellow Ltd. (UK).

TABLE II Compositions (in wt %) of the three alloys used as binders for TiB_2

Compositions	Fe	Ni	Ti	Al
FN	70	30	—	—
FNTA (1)	50.5	21.5	10.4	17.6
FNTA (2)	58.0	25.0	6.3	10.7

semi-empirical model proposed by Shetty *et al.* [11]:

$$K_{IC}^{S} = \beta\left[\frac{H(P - P_c)}{4a}\right]^{1/2} \quad (1)$$

where, P is the applied load, P_c is a threshold load before cracking is initiated, H the corresponding Vickers hardness, E the Young's modulus, β is a constant, with a value of 0.089 corresponding to the Vickers indenter geometry and "a" is the Palmqvist type crack size [12]. No cracking was observed for binder contents equal or higher than 30 vol %, even for loads applied up to 25 kg.

Direct fracture toughness measurements were carried out by the short rod, chevron-notch test method (Barker test) [13]. Test pieces were produced by HIP in rods 15 mm high and 12 mm in diameter, from which the chevron-notch geometry was machined by electrodischarge machining (EDM). Five samples were tested for each composition using an Instron test machine at an actuator speed of 0.1 mm/min. The equation used to evaluate K_{IC} was:

$$K_{ICSR} = \frac{Y^* P_{max}}{B\sqrt{W}} \quad (2)$$

where Y^* is a geometrical factor whose value is 29.21, P_{max} is the maximum applied load, and B and W are the diameter and the length of the short rod, respectively.

3. Results

3.1. Microstructures

As reported before [14], typical microstructures of TiB_2 cermets consist of TiB_2 grains surrounded by the intergranular binder phase (Fig. 1). A fine dispersion of alumina particles is present in all sintered specimens (particles in dark contrast in Fig. 1). Alumina is a product of the "*in situ*" deoxidation process that occurs during sintering. From the point of view of mechanical behaviour of TiB_2 cermets, the most important fact is that the crystallographic nature of the major component of the binder phase can be intentionally modified by controlled additions of titanium and aluminium to the powder mixtures. X-ray diffraction patterns corresponding to samples of compositions 20 vol % FN, 30 vol % FNTA (1) and 30 vol % FNTA (2) show the three possible binders that can be found in TiB_2 cermets: a combination of austenite and M_2B type iron-nickel boride for the FN alloy, a β_2 type BCC structure for the FNTA (1) alloy and a Fe-Ni-Al austenite for the FNTA (2) alloy (Fig. 2).

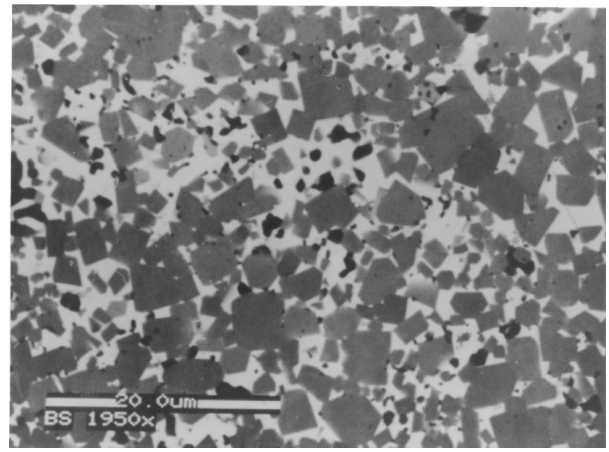

Figure 1 SEM back-scattered micrograph corresponding to TiB_2 + 20 vol % FNTA (1) binder. Alumina particles (black contrast), TiB_2 grains (grey contrast) and the metallic binder phase (white).

3.2. Hardness

Experimental results confirm that, provided that the chemical reactions are prevented, the hardness of TiB_2 cermets can be varied at ease by changing the binder volume fraction (Table III). Chemical reactions consume a non well determined part of the original TiB_2 (HV (50–200 g) = 33.7 GPa) and almost all the metallic addition by producing a softer secondary boride (M_2B HV(50–200 g) = 18.0–20.0 GPa) [1]. Therefore, the final composite hardness is difficult to predict.

Presently, a maximum hardness of 20 GPa has been achieved corresponding to the cermet containing 8 vol % of ferritic FNTA (1) binder. This value is comparable to those obtained with sub-micron WC-Co materials (Fig. 3), though the TiB_2 mean grain size obtained after sintering is about 5 microns. WC-Co data highlight the influence of the hard phase grain size on

TABLE III Mechanical properties of TiB_2 cermets

Binder composition (Table II)	Cryst. structure	Binder volume fraction (%)	σ_f (MPa)	E (GPa)	HV10 (GPa)	K_{IC} (MPa·$\sqrt{m}$)	
						Indentation test	Short rod test
FN	M_2B	20	435 ± 78	325 ± 40	16.9 ± 0.5	5.5 ± 0.8	—
		8	—	—	20.0 ± 1.0	8.2 ± 0.3	—
		14	—	—	18.7 ± 0.6	11.2 ± 0.5	9.0 ± 0.8
FNTA (1)	β_2 ferrite	20	1096 ± 70	405 ± 31	17.8 ± 0.4	12.3 ± 0.6	8.0 ± 1.0
		25	—	—	14.6 ± 1.0	15.2 ± 0.7	12.3 ± 1.5
		30	1221 ± 93	396 ± 27	14.9 ± 0.3	*	10.0 ± 1.3
FNTA (2)	austenite	30	1014 ± 90	343 ± 30	14.5 ± 0.2	*	14.4 ± 0.8

*No indentation cracks were observed.

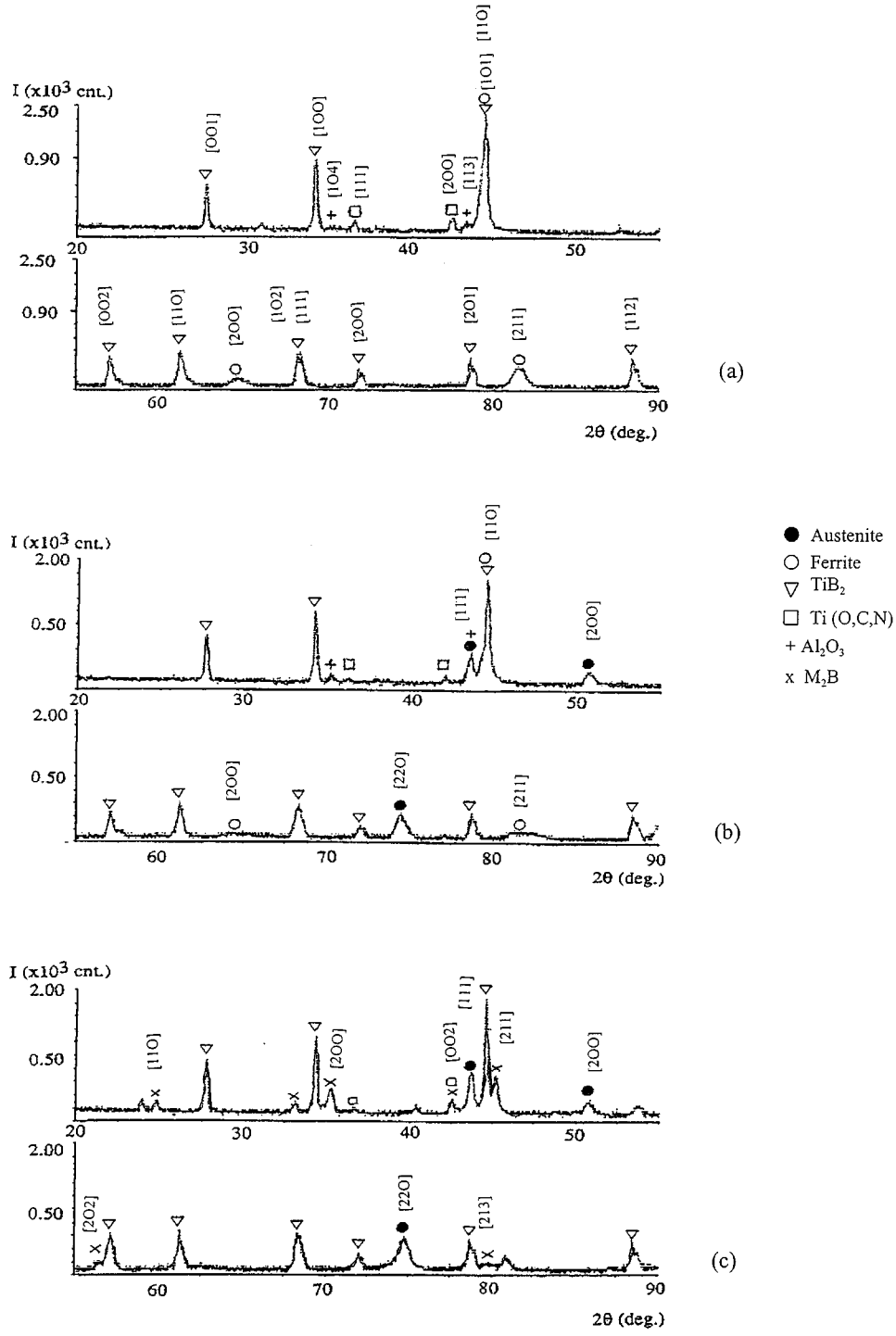

Figure 2 XRD diffraction patterns corresponding to TiB_2 cermets with 20 vol % of: (a) Ferritic binder, (b) Austenitic binder and (c) M_2B binder.

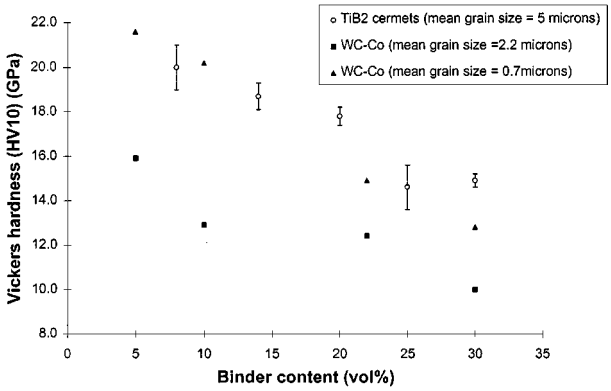

Figure 3 TiB_2 cermets. Composition FNTA (1) on Table II. Vickers hardness (HV10) vs. binder volume fraction compared to WC-Co data [15, 16].

the final cermet hardness [15, 16]. TiB_2 powders produced so far are still too coarse and these results show a potential increase in hardness out of the range covered by WC-Co materials if finer TiB_2 powders were available.

A scatter between 5 and 10% is typically observed in the hardness of TiB_2 cermets which could be attributed to the presence of a number of microstructural features, as the residual porosity and the final TiB_2 grain size. However, it must also be pointed out that an inhomogeneous binder distribution is also a source of hardness scatter.

3.3. Fracture toughness

As appreciated in Fig. 4, the expected deleterious effect of M_2B on fracture toughness of TiB_2 materials has been clearly confirmed by comparing the results obtained for TiB_2 materials with and without secondary borides. Fractographic analysis has shown that TiB_2 cermets containing metallic binders exhibit ductile fracture of the intergranular phase. The binder phase is easily identified on the fracture surface since it appears in white contrast for SEM micrographs obtained under back scattered electron detection mode (Fig. 5a). Secondary electron SEM image of the same zone (Fig. 5b) shows voiding and binder ligament area reduction to a line, both phenomena typical of plastic rupture.

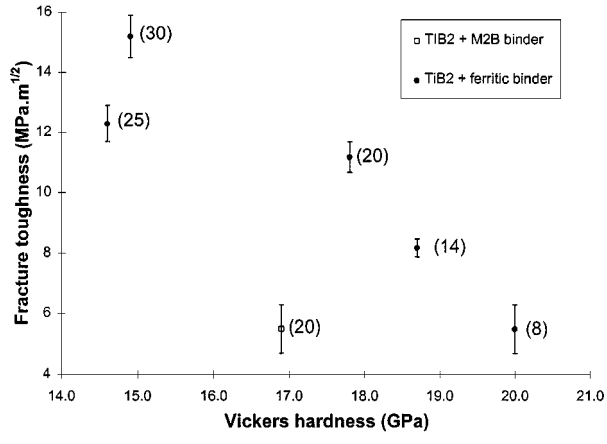

Figure 4 TiB_2 cermets. Vickers hardness vs. fracture toughness. % volume binder content of each material within brackets.

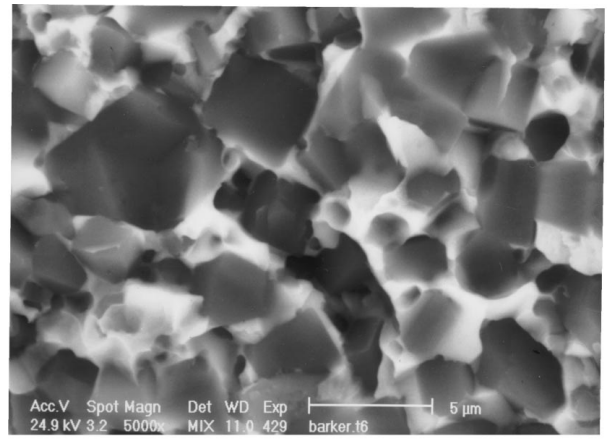

(a)

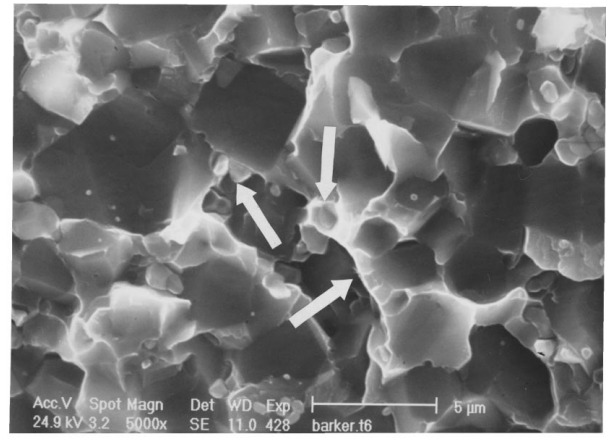

(b)

Figure 5 (a) SEM back scattered electron micrograph corresponding to $TiB_2 + 20$ vol % FNTA (1) binder showing binder location in the fracture surface (b) SEM secondary electron micrograph of the same region showing voiding and ductile rupture of the binder (see white arrows).

The overall fracture process is basically similar to that of WC-Co hardmetals [17]. Fracture of TiB_2 cermets involves four modes of rupture: cleavage of TiB_2 grains, TiB_2/TiB_2 grain boundary fracture, TiB_2/metal interfacial fracture and ductile rupture of plastic ligaments. Decohesion of the alumina-binder interface has been identified as the microstructural feature responsible for binder fracture, for alumina particles are usually found inside metal voids of the fracture surface (Fig. 6). This fact suggests that the use of powders with lower oxygen contents could increase the strength of the binder by reducing the total amount of alumina particles formed in the sintered materials.

This overall description is confirmed by the analysis of cracks produced by indentation. The result is a zone at the crack tip in which the crack has propagated through or along the boride phase, but unbroken binder phase ligaments are still bridging the gap (Fig. 7).

Quantitative estimation of the contribution of each fracture mechanism to the overall cermet fracture toughness is in progress. However, the critical role of binder plastic work on the fracture toughness of TiB_2 composites is confirmed by the extreme brittleness of TiB_2 materials with boride intergranular phases [18].

Finally, results obtained for TiB_2 with austenitic binder FNTA (2) open an alternative route for further

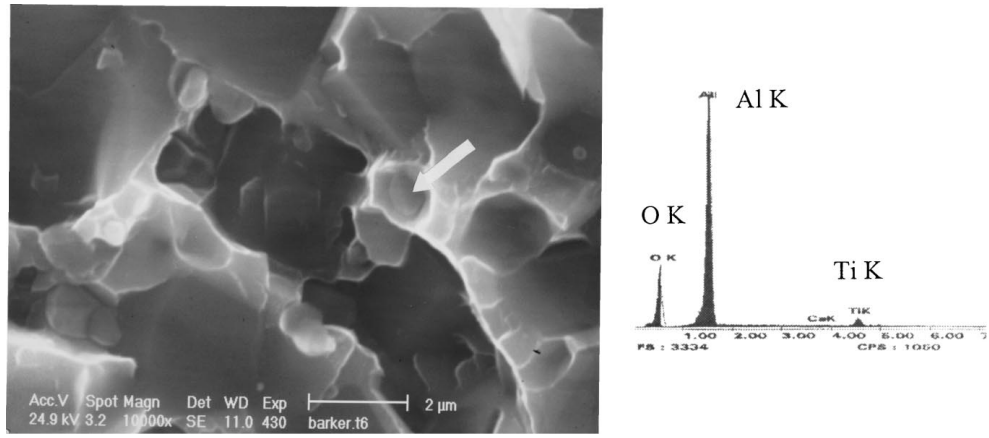

Figure 6 Detail of Fig. 5(b) showing a particle inside a metal void. The corresponding EDS analysis confirms that is alumina.

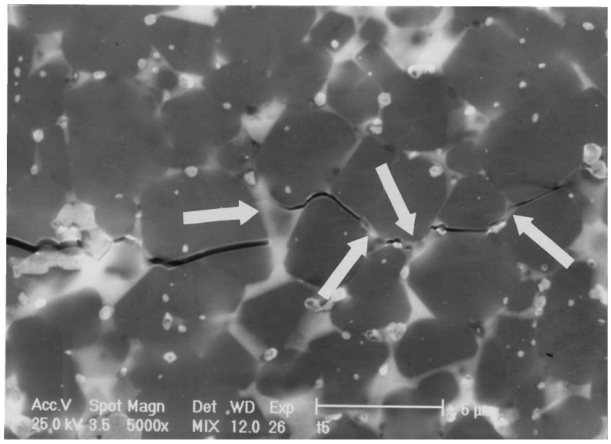

Figure 7 Composition $TiB_2 + 20$ vol % FNTA (1). Indentation crack showing metallic ligaments bridging the crack tip.

toughness improvement by the application of the transformation toughening concept [19]. XRD diffraction patterns obtained from Barker samples fracture surface (Fig. 8) have confirmed that the FNTA (2) austenitic binder is metastable and shows extensive transformation completely into martensite after testing. Correlation between transformation and K_{IC} increase is a subject of current research. However, preliminary results (Table III) prove that the metastable binder has higher fracture toughness than the ferrite based material. The martensitic transformation is believed to be activated by the stress field of a propagating crack. The additional energy required for such transformation is obtained from the stress field surrounding the crack tip. Therefore, the driving force for crack growth is reduced.

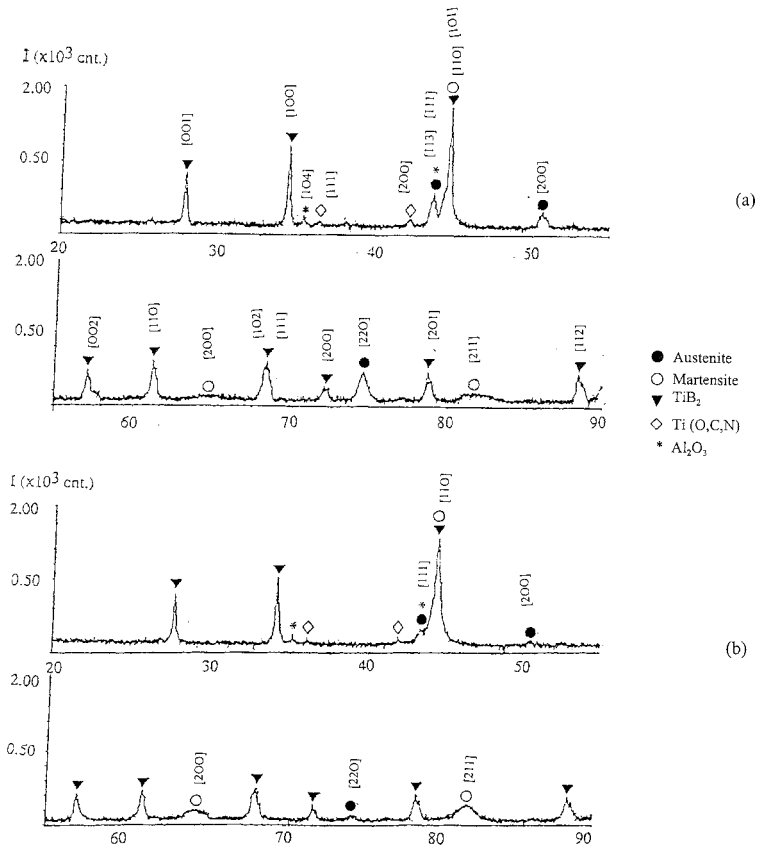

Figure 8 Composition $TiB_2 + 30$ vol % FNTA (2). XRD diffraction patterns corresponding to the fracture surface of Barker test pieces: (a) before testing and (b) after testing.

4. Conclusions

TiB_2 based cermets are ultra hard materials with mechanical properties comparable those of the best grades of conventional hardmetals (HV10 ≈19 GPa and $K_{ICSR} \approx 9$ MPa·$\sqrt{m}$). These results constitute a significant improvement with respect to TiB_2 composites produced so far. As described in this work, the plastic behaviour of the metallic binder phase during fracture is responsible for the increase in fracture toughness observed in these materials. It has also been shown that metastable austenitic binder phases provide an additional increase in fracture toughness through a transformation toughening mechanism. Additionally, close control of the chemical composition of the metallic binder is critical to avoid brittle intergranular phases which lead to extremely brittle materials.

Acknowledgements

The authors gratefully acknowledge the financial support of the European Committee through the BRITE-EURAM Project BE96-3356, "ULTRA HARD MATERIALS FOR TRIBOLOGICAL APPLICATION (ULTRATRIBO)," (Contract No. BRPR-CT96-0304), for the realisation of this work.

References

1. P. A. DEARNLEY and T. BELL, *Surface Engineering* **1** (3) (1985) 203.
2. S. BAIK and P. F. BECHER, *J. Amer. Cer. Soc.* **70** (8) (1987) 527.
3. J. D. KATZ, R. D. BLAKE and C. P. SCHERER, *Ceram. Eng. Sci. Proc.* **10** (7-8) (1989) 857.
4. G. V. SAMSONOV, *Met. Obra. Metall.* **1** (1958) 35.
5. H. PASTOR, in "Boron and Refractory Borides," edited by V. I. Matkovich (Springer-Verlag, Berlin, 1955) p. 457.
6. J. M. SÁNCHEZ, M. G. BARANDIKA, J. GIL SEVILLANO and F. CASTRO, *Scr. Metall. Mater.* **26** (1992) 957.
7. H. PASTOR, C. ALLIBERT, M. G. BARANDIKA, J. M. SÁNCHEZ, J. GIL, M. FUENTES and F. CASTRO, Int. Conf. on Advances in Hard Materials Production, Bonn, (1992), p. 135.
8. H. PASTOR, C. H. ALLIBERT, M. L. OTTAVI, M. ALBAJAR and F. CASTRO, Patent no. 91 08030, Paris (1991).
9. M. G. BARANDIKA, J. M. SÁNCHEZ and F. CASTRO, *Metal Powder Report* **2** (1994) 49.
10. F. CASTRO and I. ITURRIZA, *J. Mater. Sci. Lett.* **9** (1990) 600.
11. K. SHETTY, I. G. WRIGHT, P. N. MINCER and A. H. CLAUER. *J. Mater. Sci.* **20** (1985) 1873.
12. J. M. SÁNCHEZ, Doctoral thesis, University of Navarra, 1993, p. 91.
13. ASTM Designation E 1304-89, 962 (1990).
14. M. G. BARANDIKA, J. M. SÁNCHEZ, T. ROJO, R. CORTÉS and F. CASTRO. *Scripta. Materialia.* **39** (10) (1998) 1395.
15. M. T. LAUGIER, *Acta metall.* **33** (11) (1985) 2093.
16. L. J. CHERMANT and F. OSTERSTOCK, *J. Mater. Sci.* **11** (1976) 1939.
17. J. HONG and J. GURLAND, in "Science of Hard Materials," edited by R. K. Viswanadham, D. J. Rowcliffe and J. Gurland (Plenum Press, New York, NY, 1983) 649.
18. R. TELLE and G. PETZOW, *Mater. Sci. and Eng.* **A105/106** (1988) 97.
19. R. K. VISWANADHAM and P. G. LINDQUIST, *Metall. Trans.* **18A** (1987) 2163.

Received 3 March
and accepted 15 July 1999